



# On-line measurement of fluorescent aerosols near an industrial zone in the Yangtze River Delta region using a wideband integrated bioaerosol spectrometer

Yan Ma<sup>a,1</sup>, Zhibin Wang<sup>b,1</sup>, Dongsen Yang<sup>a</sup>, Yiwei Diao<sup>a,c</sup>, Weiwei Wang<sup>c</sup>, Hongliang Zhang<sup>d</sup>, Wenhui Zhu<sup>a</sup>, Jun Zheng<sup>a,\*</sup>

<sup>a</sup> Collaborative Innovation Center of Atmospheric Environment and Equipment Technology, Nanjing University of Information Science & Technology, Nanjing 210044, China

<sup>b</sup> Research Center for Air Pollution and Health, College of Environmental and Resource Sciences, Zhejiang University, Hangzhou 310058, China

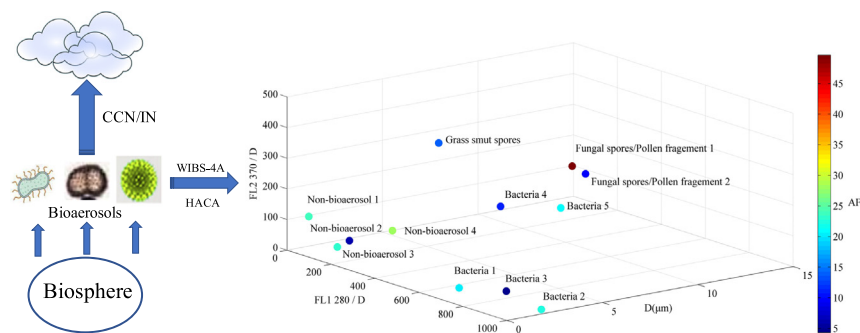
<sup>c</sup> Key Laboratory for Aerosol-Cloud-Precipitation of China Meteorological Administration, Department of Atmospheric Physics, Nanjing University of Information Science and Technology, Nanjing 210044, China

<sup>d</sup> Handix Scientific LLC, Boulder, CO 80301, USA

## HIGHLIGHTS

- Bioaerosols only accounted for <1% of the total WIBS-4A signals.
- WIBS-4A combined with cluster analysis may be an effective way to identify bioaerosols.
- Bacteria, fungal spores and/or pollen fragments were the dominant bioaerosols in Nanjing.
- Bioaerosols may present complex size-distributions and morphology.

## GRAPHICAL ABSTRACT



## ARTICLE INFO

### Article history:

Received 12 October 2018

Received in revised form 21 November 2018

Accepted 24 November 2018

Available online 26 November 2018

Editor: Jianmin Chen

### Keywords:

Primary biological aerosol

WIBS-4A

Cloud condensation nuclei

Ice nuclei

Hierarchical agglomerative cluster analysis

## ABSTRACT

In this work, we present on-line fluorescent aerosol measurements by the wideband integrated bioaerosol spectrometer (WIBS-4A) near an industrial zone in Nanjing, a megacity in the Yangtze-River-Delta (YRD) region. The fieldwork was conducted from April 1 to May 8, 2014. A TSI 3321 aerosol-particle-sizer (APS) was simultaneously deployed to measure the total number size distribution of aerosol with diameter from 0.8–20 μm. Both WIBS-4A and APS reported similar number concentration and temporal profiles ( $R^2 = 0.72$ ). However, the daily average number of potential bioaerosols was only  $0.5 \pm 0.2\%$  of the total particles detected by the WIBS-4A and displayed a completely different diurnal profile from that of APS. In addition, WIBS-4A can only provide integrated fluorescent signals, which strongly limited the potential to specifically identify the bioaerosols. Accordingly, hierarchical-agglomerative-cluster-analysis (HACA) was utilized to identify and speciate the potential bioaerosols from the WIBS-4A dataset. By maximizing the total distances among all potential cluster centers, a 12-cluster solution was accepted as the optimum result. These clusters were further identified according to their fluorescent signatures, size, and morphology, i.e., non-bioaerosols, bacteria, and fungal spores and/or pollen fragments. Bacteria were the dominant bioaerosol species detected in this work. The diurnal profiles of bioaerosols correlated very well with relative humidity (RH), reaching daily maxima around 3 AM–6 AM,

\* Corresponding author at: School of Environmental Science and Engineering, Nanjing University of Information Science & Technology, Nanjing 210044, China.

E-mail address: [zhengjun@nuist.edu.cn](mailto:zhengjun@nuist.edu.cn) (J. Zheng).

<sup>1</sup> Contributed equally to this work.

indicating the presence of humidity controlled bioaerosol emission mechanism, i.e., bacteria may flourish under moderate ambient temperature, RH, and the absence of UV radiation. The size- and AF-distributions of bioaerosols indicated that bioaerosols normally varied substantially in size and assumed a rather irregular shape. Although the number concentration of bioaerosols was relatively small, most bioaerosols can efficiently serve as ice nuclei by providing rough and irregular surfaces, verified by the observation results. Therefore, WIBS-4A measurements can still be informative for investigations of bioaerosols in the atmosphere, especially when HACA method was incorporated into the data processing.

© 2018 Elsevier B.V. All rights reserved.

## 1. Introduction

Primary biological aerosols (PBAs) or bioaerosols represent a relatively small but unique subset of primary aerosols. Unlike inorganic salts and organic aerosols, bioaerosols are poorly characterized. Their number concentrations, size-distributions, morphology, types, and sources are not well known. Bioaerosols are generally regarded as aerosols originated from biological organisms, comprising both live microorganisms and debris of biological materials (Després et al., 2012; IGAP, 1992; Poschl and Shiraiwa, 2015). Although bioaerosols are essentially made up of organic compounds, they should be differentiated from secondary organic aerosols (SOAs), which are mostly formed from photochemical oxidation products of volatile organic compounds (VOCs) of either biogenic or anthropogenic origins. Commonly observed bioaerosols include viruses, bacteria, fungal spores and pollens (Poschl and Shiraiwa, 2015). The reported size of bioaerosols can range from as small as a few nanometers to hundreds of micrometers, such as plant debris (Poschl, 2005). Despite its biological origin, bioaerosols can function as typical atmospheric aerosols, i.e., affecting regional and global climate by directly interacting with solar/terrestrial radiation or by acting as cloud condensation nuclei (CCN) to participate in cloud formation (Després et al., 2012; Poschl, 2005; Poschl et al., 2010). Furthermore, bioaerosols are often found in the coarse mode and thus can form larger cloud droplets at lower supersaturations, i.e., “giant CCN” (Pope, 2010). Especially, bioaerosols have been suggested to be the most important ice nuclei (IN) in clouds warmer than  $-15\text{ }^{\circ}\text{C}$  (Demott and Prenni, 2010). Some bioaerosol, such as pollen, may be activated as heterogeneous IN at  $-5\text{ }^{\circ}\text{C}$  or lower (Diehl et al., 2002). Therefore, bioaerosols could play an important role in regulating global precipitation and hydrological cycle (Després et al., 2012), particularly in pristine environment (Poschl et al., 2010; Poschl and Shiraiwa, 2015).

Bioaerosols also exert severe threats to human health (Després et al., 2012). Bioaerosols not only can serve as carriers of toxic materials including carcinogens, but also are pathogen of infectious diseases themselves, such as viruses and bacteria, which can be suspended in air for weeks. Fungi spores and pollens are particularly well known to cause allergic diseases, especially to the respiratory tracts, such as asthma and bronchitis (Reid and Gamble, 2009). Under polluted conditions, biogenic substances may react with ozone ( $\text{O}_3$ ) and nitrogen oxides ( $\text{NO}_x$ ) to form reactive oxygen intermediates and nitrated proteins that can intensify immune system reactions and aggravate allergic diseases.

Comparing to non-biological aerosols, PBAs measurements are usually not included in field studies and hence relatively little is known about their ambient concentration, number-size distribution, identities, spatial variation, and seasonality, which are affected by meteorological factors, anthropogenic activities, variability of emission sources, and many other complicated variables (Després et al., 2012). Bioaerosol detection techniques are rather limited to off-line analysis, which normally takes hours and days to complete and this is partially responsible for the fact that bioaerosols are seldom studied in field campaigns. Traditionally, bioaerosols are primarily measured by off-line techniques, i.e., samples are collected by impaction onto substrates followed by analyses with optical and electron microscopy (Cox and Wathes, 1995). To detect specific viable samples, cultivation is also needed. Light microscopic technique is

the first and the most widely used PBAs analysis method, which is useful to detect bioaerosols larger than  $2\text{ }\mu\text{m}$ , such as pollen. Similarly, fluorescence microscopy is a routine method to obtain the total count of microorganism by observing the fluorescence of samples after fluorescent dye labeling. Since certain dye will fluorescence different color when binds to certain function group of bioaerosols, fluorescence microscopy can provide some selectivity in determining the types of bioaerosols. However, counting bioaerosols using microscopy methods is rather tedious, time-consuming, and subject to human errors. Hence, it cannot be used for on-line analysis of bioaerosols, especially to provide high time-resolution observations. Other methods have been developed to assess the abundance of PBAs, such as using chemical tracers, e.g. mannitol and arabinol can be used as proxies of fungal spores. Genetic materials (DNA and RNA) comprise substantial portion of bioaerosols and can be used as unique signatures of microorganisms for the purpose of both identification and quantification. But extraction and analyses of generic material require complicated pretreatment of the samples, which it impossible for in-situ measurements.

The development of on-line bioaerosols measurement techniques benefits from the research in fast-detection of bio-warfare agents (Kaye et al., 2000). Bioaerosols often contain substantial heterocyclic aromatic compounds or molecules with conjugated double bonds, which are efficient fluorophores, such as amino acids (e.g. tryptophan, tyrosine, and phenylalanine) and coenzymes (e.g. flavins and vitamin B6 and B9) (Pöhlker et al., 2012). Thus, light-induced fluorescence or auto-fluorescence can be used to detect bioaerosols. There are two commercialized instruments that are available to do on-line PBAs measurements, i.e., the ultraviolet aerodynamic particle sizer (UV-APS, TSI Inc.) (Hairston et al., 1997) and the wide issue bioaerosol sensor (WIBS) developed by the University of Hertfordshire (Kaye et al., 2000). UV-APS is similar to a normal APS, which can deduce the aerodynamic diameter of a particle from the time it spends to pass through two laser beams. Additionally, UV-APS can also measure bioaerosols' fluorescence intensity from  $420\text{ nm}$ – $575\text{ nm}$  after excitation by a  $355\text{-nm}$  pulsed laser. WIBS is more sophisticated than a UV-APS. WIBS not only can provide particle size information but also can assess particle morphology by measuring the scattered laser signals. More importantly, WIBS are equipped with two excitation UV flash lamps, i.e.,  $280\text{ nm}$  and  $370\text{ nm}$ , and the fluorescent emissions are measured at  $310$ – $400\text{ nm}$  and  $420$ – $650\text{ nm}$ , respectively. Therefore, WIBS datasets are more informative in terms of bioaerosol identifications. One typical measurement cycle of WIBS is about  $25\text{ }\mu\text{s}$  but the actual sampling rate is limited by the flash rate of the UV lamp ( $125\text{ Hz}$ ). The performance of WIBS has been evaluated comprehensively and successfully by both laboratory tests and field studies (Healy et al., 2012a; Healy et al., 2012b; O'Connor et al., 2014; O'Connor et al., 2013; Toprak and Schnaiter, 2013). Nevertheless, WIBS has been demonstrated to be a fast-response and highly sensitive bioaerosol/fluorescent aerosol sensor.

Interpretation of the WIBS dataset is a challenging task due to the diversity of bioaerosols in the atmosphere and is made more difficult by WIBS's fast sampling rate. Classification is a prerequisite to fully comprehend WIBS datasets. Since in most cases the identities of bioaerosols are unknown, an idea classification method should be subject to all possibilities without any bias. Hierarchical agglomerative cluster analysis (HACA)

is such an objective statistic method that does not require any assumption of the number of types and the relative abundance of bioaerosols in the target area. Average-linkage algorithm (ALA) is often used in HACA for its flexibility in different group size (Everitt, 1993). Initially, each data point is considered as a single-membered cluster in HACA. Then, a data pair with the minimum Euclidian distance will be agglomerated into one cluster, and so on. The final goal to achieve is that the Euclidian distance within any cluster is minimized but the Euclidian distance between any two clusters are maximized. The only drawback of HACA is that the computer processing time increases with the square of the size of the dataset and it requires impractical amount of physical memory to store and process a large dataset (e.g. >10,000 particles).

Despite the advancement in bioaerosol measurement and analysis techniques, on-line observation of PBAs is seldom conducted during air quality research, especially in China. Consequently, our knowledge of the underlying mechanisms that dominate the interaction between bioaerosols and atmospheric processes are still very limited and characterization of bioaerosols in model simulations is poorly constrained. For example, the estimated global average emission rates of fungal spores can vary by about one order of magnitude (Després et al., 2012) and their ambient concentration may be determined by some humidity-controlled release mechanisms (Toprak and Schnaiter, 2013).

Only recently, Yu et al. (2016) have reported a short period (~2 weeks) of fluorescent aerosol measurement at a rural site in the YRD region. Since the measurements were conducted in late autumn, combustion processes, such as biomass burning, very likely contributed most of the fluorescent aerosols (Yu et al., 2016). In this work, we conducted bioaerosol measurements during springtime (the most flourishing season of a year) at a suburban site in Nanjing China using a wideband integrated bioaerosol spectrometer model 4A (WIBS-4A, Droplet Measurement Technologies, USA), which was developed from the original wide issue bioaerosol sensor (Healy et al., 2012b). Major types of fluorescent aerosols were identified using HACA and their temporal variation and the potential affecting factors were investigated.

## 2. Experimental methods

### 2.1. Field measurements overview

The measurements were conducted at a meteorology observatory facility (N32.2058°, E118.7053°) located on the campus of Nanjing University of Information Science and Technology (NUIST) (Zheng et al., 2015) and the observation period was from 1 April to 8 May 2014. The site was about 15 km to the north of the urban center and was surrounded by agriculture lands and residential areas. From previous work, this site has been demonstrated to be occasionally affected by local industrial emissions, such as formaldehyde (Ma et al., 2016) and amines (Zheng et al., 2015). The WIBS-4A instrument was housed inside an air-conditioned trailer, which was placed on a glass land along with other meteorology observation instruments. To minimize the inlet length, the WIBS-4A was positioned on a 1.8 m tall shelf. A ~80 cm long, 10 mm OD stainless steel tubing was used as an inlet, which was installed vertically up through the trailer roof. About 10 cm above the inlet was a 15 cm diameter stainless steel funnel to shield the inlet from precipitations. The sampling inlet was about 0.6 m above the trailer roof and ~3 m above the ground. No taller buildings and trees were within ~40 m radius of the trailer.

### 2.2. WIBS-4A

The WIBS-4A was manufactured and fully characterized by the Droplet Measurements Technologies (Healy et al., 2012a; Healy et al., 2012b; Toprak and Schnaiter, 2013). WIBS-4A was basically a single-particle fluorescence sensor, comprising a laminar-flow delivery system and a central optical chamber equipped with a continuous-wave 635 nm diode laser source, a forward-scattering quadrant

photomultiplier tube (Q-PMT), two pulsed Xenon UV sources (Xe1 and Xe2 for 280 nm and 370 nm excitation, respectively), and two fluorescence detection channels, i.e., FL1 (310–400 nm) and FL2 (420–650 nm). In operation, about 2.5 L min<sup>-1</sup> air sample was sucked into the WIBS-4A and ~2.2 L min<sup>-1</sup> of the total airflow was deflected into a HEPA filter to form a sheath flow around the remaining sample flow, within which particles were confined into a single file before entering the optical chamber. Firstly, any particle will pass through the continuous-wave 635 nm laser beam. The side-scattered light was captured by FL2 channel and its intensity was converted to the size of the particle using Mie theory under the assumption that the particle was spherical and had the same refractive index as polystyrene latex (PSL) spheres (1.58), which were used for size calibrations. In this work, the size calibration function was deduced from a polynomial fit of the FL2 channel signals corresponding to nebulized 2.0, 2.8, and 5.1 μm PSLs, respectively (see Fig. A.1). The forward-scattered light from the particle was collected by the Q-PMT and was used to assess particle shape with a value ranging from 0 (spherical) to 100 (rod-shaped), i.e., asymmetry factor (AF). If the particle was bigger than 0.5 μm as determined by the side-scattering intensity, Xe1 and Xe2 will be sequentially fired with ~10 μs apart. The resulting fluorescence signals were recorded as FL1\_280/FL2\_280 and FL2\_370, respectively. Since Xe2 emission was within the FL1 detection wavelength range, only FL2 signal was valid after firing Xe2. For each particle, the measurement cycle was about 25 μs. However, the maximum firing rate of the Xenon flash-tube was about 125 flashes s<sup>-1</sup>. Correspondingly, the maximum particle number concentration can be accurately detected was about ~2.5 × 10<sup>4</sup> L<sup>-1</sup>. In this work, WIBS-4A was operated at a preset “High Gain” mode with a detection size range of 0.5 μm ~ 15 μm. Since most bioaerosols were found larger than 0.8 μm, only particles larger than 0.8 μm were considered as potential bioaerosols in this work. The background fluorescence signals were checked every 2 h for 5 min by stopping the sample flow and firing the Xe lamps.

### 2.3. APS and meteorology measurements

A TSI model 3321 aerodynamic particle sizer (APS) was used to measure the number-size distribution of aerosol with an aerodynamic diameter of 0.5–20 μm. The inlet of the APS was also made of a 2 m long 10 mm OD stainless steel tubing. No diffusion driers were used in the sampling lines of both the WIBS-4A and the APS. In order to inter-compare with the WIBS-4A data, only particles larger than 0.8 μm measured by the APS were considered here.

Meteorological parameters, including wind-direction, wind-speed, temperature, pressure, solar radiation, relative humidity, and precipitation were measured by the nearby weather station maintained by the Chinese National Meteorology Bureau according to Chinese national standard GB31221–2014.

### 2.4. Hierarchical agglomerative cluster analysis

During initial test runs, we found that majority of the raw data points (>70%) were detected with relatively low fluorescence intensities, i.e., FL1\_280 = 10 ± 3.7, FL2\_280 = 16 ± 1.3, and FL2\_370 = 8 ± 0.8, which were thus considered as non-fluorescent particles (Robinson et al., 2013) and excluded from further HACA. The total number of fluorescent data points collected each day ranged from ~600,000 to ~800,000.

HACA was critically limited by the capacity of the physical memory of the computer. In this work, a subset (~1% or ~8000 particles) of the total data was randomly chosen from a 24-h validated dataset. Each data point was treated as a five-membered vector (FL1\_280, FL2\_280, FL2\_370, size, AF). Since both particle size and AF were log-normally distributed, the log-values of size and AF were used in the analysis. The HACA was performed with the IBM SPSS 19.0 software package using averaged linkage algorithm. The number of clusters tested ranged from 2 to 28. The distance between any two clusters ( $L_{A,B}$ ) was defined

as Eq. (E1),

$$L_{A,B} = \frac{1}{mn} \sum_{i=1}^m \sum_{j=1}^n \|A_i - B_j\|^2 \quad (\text{E1})$$

i.e., the average squared Euclidian distance between all pairs of particles, one from each cluster, where  $A_i$  and  $B_j$  respectively represented one data vector from  $m$ - and  $n$ -membered clusters. The pair of clusters with the minimum distance was considered the most similar clusters. The optimum number of clusters ( $N$ ) was determined by evaluating two indicators, i.e., the normalized coefficient of determination ( $R^2$ ) (Eq. (E2)) and the root mean squared (RMS) distance between all pair of clusters (Eq. (E3)) (Robinson et al., 2013).

$$R^2 = 1 - \frac{\text{Sum of squares within clusters}}{\text{total sum of squares}} \quad (\text{E2})$$

$$\text{RMS} = \sqrt{\frac{\sum_{A=1, B=A+1}^{N-1, N} (L_{A,B})^2}{N(N-1)/2}} \quad (\text{E3})$$

When two dissimilar clusters were combined together, the sum of squares or distance within the cluster will increase dramatically, which will lead to significant decrease in  $R^2$  but a substantial increase in RMS. The proper number of clusters was hence determined. The rest of the data points were classified into these clusters according to their shortest distance ( $d_i$ ) to the centers of these clusters (Eq. (E4)),

$$d_i = \left| \frac{c_i - p}{\sigma_i} \right| \quad (\text{E4})$$

where  $c_i$  was a 5-membered position vector pointing to the center of cluster  $i$ ,  $p$  was the to be classified data point,  $\sigma_i$  was the vector consisting of the standard deviations of each of the five measured variables within cluster  $i$ . The number of bioaerosol in each cluster was also recorded accordingly.

## 2.5. WIBS-4A data processing procedure

The WIBS-4A dataset was processed as described by the flow chart shown in Fig. A.3. The raw data collected by the WIBS-4A was firstly filtered by its signal intensity, i.e., it must be higher than the background signal (fluorescence signal threshold  $+3\sigma$ ) to be qualified as fluorescent particles for further analysis. Five separate sub-datasets (~8000 data points each) without precipitation or other extreme weather conditions were then randomly selected from five typical observation days that scattered throughout the campaign period and were independently processed using the HACA to identify the number of major clusters, i.e., the potential major types of bioaerosols. At last, the distances between each validated data point and the cluster centers were calculated using Eq. (E4) and accordingly the data point was assigned to the cluster with the minimum distance from it.

## 3. Results and discussion

### 3.1. General observation

Fig. 1 shows the time series of bioaerosols, total number of particles measured by WIBS-4A, non-fluorescent particles, and number of particles detected by FL1\_280, FL2\_280, and FL2\_370 channels during the observation period, respectively. Also shown in Fig. 1 are the meteorology parameters, including RH, temperature ( $T$ ), wind speed, and solar radiation

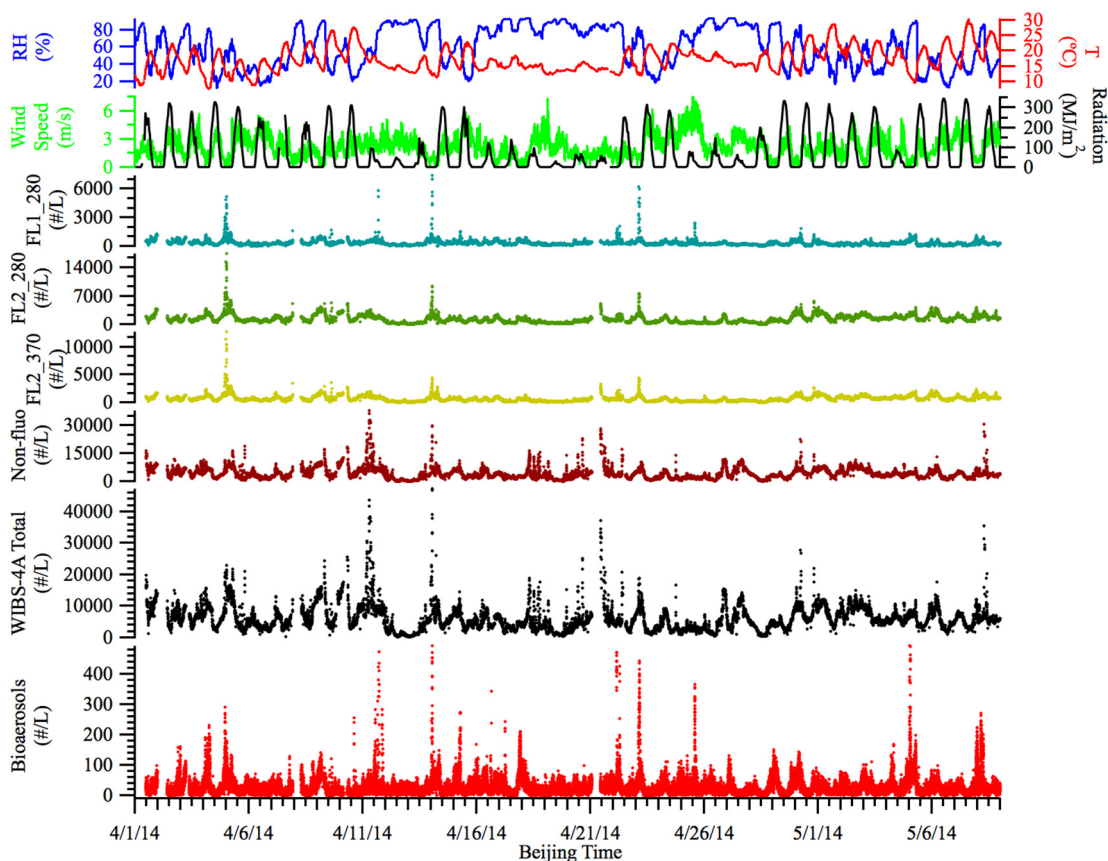


Fig. 1. Time series of bioaerosols, total number of particles measured by WIBS-4A, non-fluorescent particles, and number of particles detected by FL1\_280, FL2\_280, and FL2\_370 channels, respectively, along with meteorology parameters (RH, Temperature, Wind speed, and solar radiation). The bioaerosol data is retrieved from hierarchical agglomerative cluster analysis.

radiation intensity. Evidently, the WBS-4A data set is dominated by non-fluorescent particles, indicated by the similarity between the profiles of non-fluorescent and WBS-4A total concentration. In fact, the profiles of APS data and the total signals measured by WBS-4A were significantly similar to each other (see Fig. A.2a) with a correlation coefficient of 0.72 (Fig. A.2b). However, after filtering out the non-fluorescent particles according to the aforementioned criteria, the daily potential bioaerosol concentration classified by the HACA only accounted for a small portion of the WBS-4A total, ranging from 0.13% to 1.2% with an average of  $0.5 \pm 0.2\%$ . In general, bioaerosol concentration was found below  $\sim 100 \text{ \# L}^{-1}$  but occasionally can reach maxima of  $\sim 500 \text{ \# L}^{-1}$ . Bioaerosols also showed clear diurnal variations reaching the lowest concentration at noon and the highest concentration around 3 AM to 6 AM. After sunrise, bioaerosols decreased swiftly and reached the daily minimum around noon, which was most likely due to the germicidal effects of sunlight. It also showed that in sunny days (e.g., 29 April to 3 May), diurnal profiles were more distinguishable and the magnitude of daily variation was larger than rainy days (e.g., April 19 to 21). However, most of the bioaerosol peak events with the extreme values (e.g., around midnights of April 11, 13, 22, and May 4) were all preceded by a cloudy day or precipitation event. This may due to the fact that bioaerosols, especially in the cases of bacteria and fungi, were favored by humid and dark conditions.

To further investigate the effects of the ambient environment on bioaerosols, Fig. 2 shows the 24-h averaged diurnal profiles of bioaerosols, RH, temperature, and solar radiation flux. Evidently, bioaerosols correlate very well with RH (see Fig. A.4 up). Since RH was mainly decided by the ambient temperature, bioaerosols also anti-correlated well with temperature (Fig. A.4 down). It was very typical to experience high humidity in early morning during springtime and normally varied around 70%. Meanwhile, temperature was around 15 °C and solar radiation was negligible. Under these conditions, bacteria or fungi can proliferate substantially, although  $\sim 20 \text{ °C}$  would be ideal

for the reproduction of microorganisms. The surrounding of the site was covered by grassland, which can serve as an ideal habitat for bioaerosols to survive. Additionally, in the early morning, although temperature already started increasing, sunlight was still too weak to cause significant damage to the bioaerosols. Right after that, temperature increased quickly along with solar radiation, strengthened vertical convection can lead to substantial decrease of bioaerosol concentration, which would be further suppressed by the deadly and ever-increasing UV radiation. In the afternoon, both dry weather condition and strong solar radiation were adverse for bioaerosols to survive. After sunset, vertical mixing was weakening and solar radiation disappeared, suitable for the reproduction and accumulation of bioaerosols.

Precipitation can affect bioaerosol concentration in several aspects. In one sense, heavy rainfall can wash out bioaerosols just like other typical atmospheric aerosols through wet deposition. In addition, the low temperature concurred with the precipitation was unfavorable for the reproduction of bioaerosols. However, bioaerosols within the rain droplets may be re-suspended into the atmosphere when they splashed onto any hard surfaces, e.g., ground or building surfaces (Heo et al., 2014). In addition, weak solar radiation and humid air during precipitation and cloudy days can counteract the wet deposition effects to some extent. Consequently, the diurnal variation of bioaerosols during precipitation days was suppressed. However, these moderate weather condition may provide suitable moisture and other prerequisites for the blooming of bioaerosols in the following days.

### 3.2. Potential interferences

In principle, compounds with conjugated double bonds are efficient fluorescence emitter, such as polycyclic aromatic hydrocarbons (PAH) and humic-like substance (HULIS). Soot particles generated from incomplete combustion processes may absorb fluorescent compounds

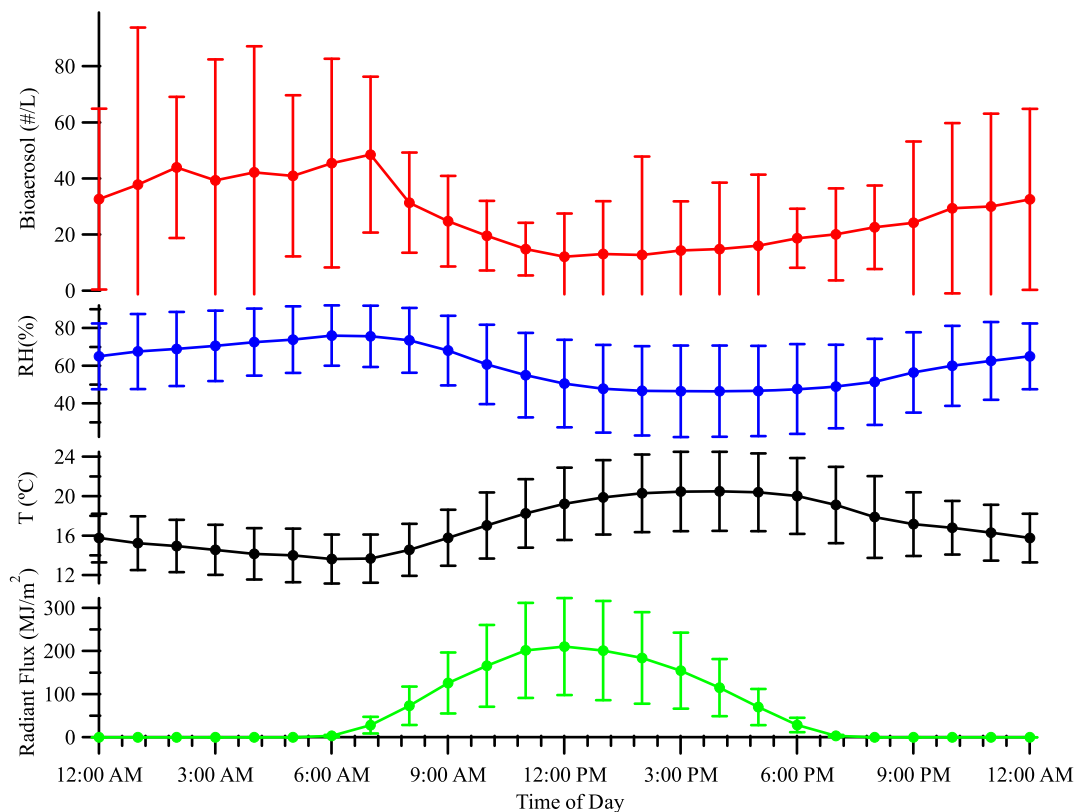


**Fig. 2.** Diurnal variations of bioaerosols (red), RH% (blue), ambient temperature (black), and solar radiation flux (green). RH appears to be the dominating factor that controls bioaerosol emission.

such as PAH and nitrogen-substituted heterocyclic aromatic compounds, and they can become extrinsic fluorescent. However, freshly emitted soot particles are often in the accumulation mode (Cross et al., 2010) and their fluorescence are found relatively weak due to inner quenching effects (Panne et al., 2000). Typical abundance of HULIS in  $PM_{10}$  is on the order of a few  $\mu g m^{-3}$  in urban environment (Zheng et al., 2013) and the fluorescent intensities of HULIS are found extremely weak (Pöhlker et al., 2012). To minimize the potential interference from non-biological fluorescent aerosols, any sample with a diameter  $<0.8 \mu m$  and fluorescent intensities of three channel respectively  $<10 + 3.7$ ,  $16 + 1.3$ , and  $8 + 0.8$  was considered as a non-fluorescent aerosol (i.e., non-biological aerosols) and was excluded from further analysis.

### 3.3. Determination of types of bioaerosol

The major types of potential bioaerosols from the remaining fluorescent aerosols were determined by the HACA method as described above. Due to the limitation of the calculation capacity, HACA can only be applied to one-day-dataset each time. To demonstrate the consistency of the analyses results and to be more representative, five separate days without precipitation events (April 9, 15, 22, 30, and May 5) from each week of the observation period were chosen to perform the HACA. The time interval between any two adjacent sample days ranged from 6 to 8 days to account for possible dramatic changes of air masses that might bring different types of bioaerosols onto the site. Fig. 3 shows the plots of normalized  $R^2$ , RMS, and the number (N) of

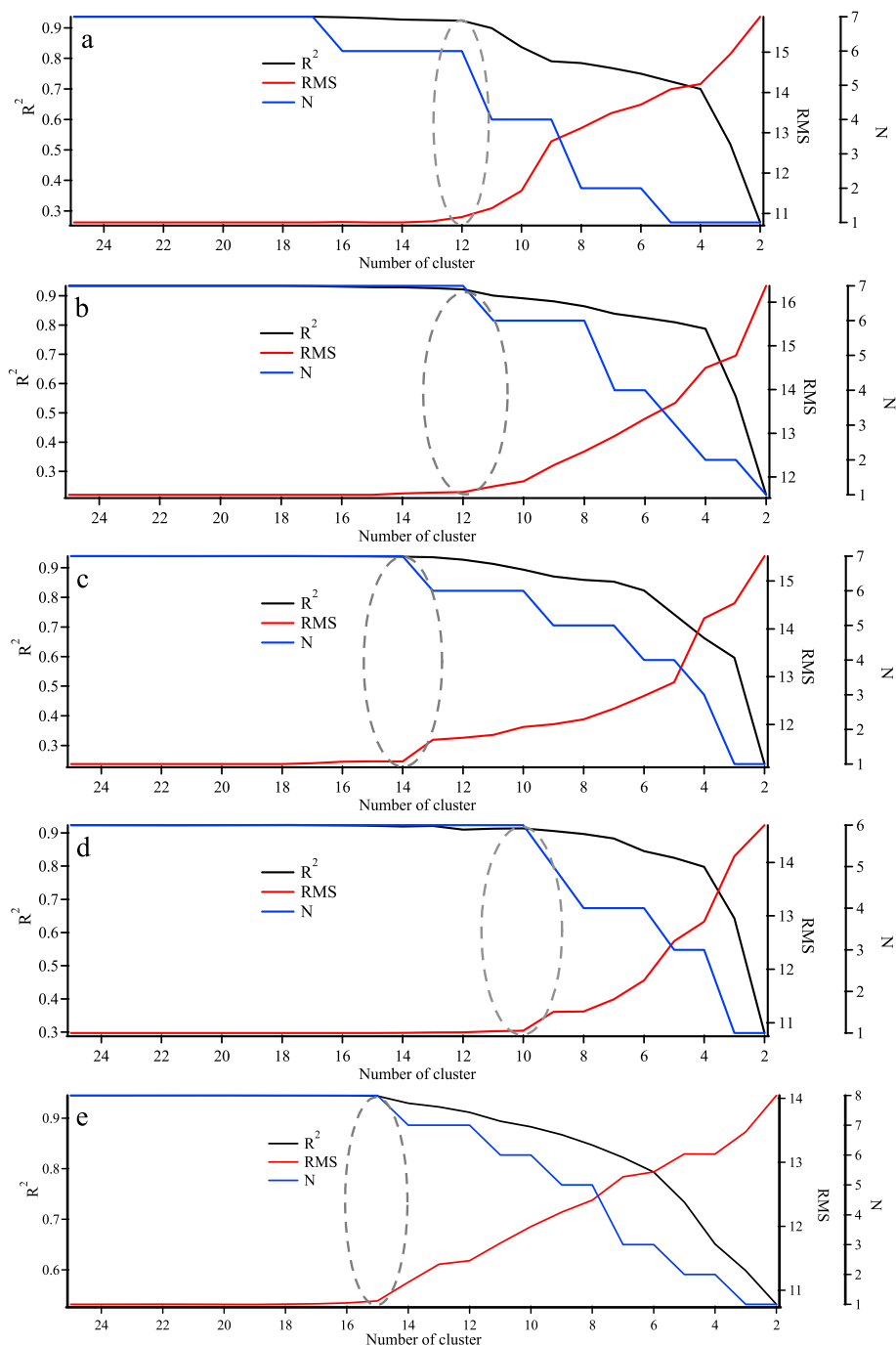


**Fig. 3.** Average-linkage statistics of normalized  $R^2$ , RMS, and the number (N) of major clusters (i.e., any cluster with a population more than half of the average cluster size) for a) April 9, b) April 15, c) April 22, d) April 30, e) May 5, respectively. The oval shapes indicate the optimum number of clusters.

**Table 1**

The types of PBA classified according to the HACA method and their characteristic signals.

CLUSTER#	Type of PBA	FL1_280	FL2_280	FL2_370	SIZE ( $\mu\text{m}$ )	AF	Total counts
1	Non-bioaerosol-1	18.1	92.6	93.8	0.9	23.8	$7.7 \times 10^6$
2	Non-bioaerosol-2	171.9	98.1	45.4	2.5	5.9	$5.3 \times 10^6$
3	Non-bioaerosol-3	149.2	103.3	25.8	1.4	22.8	$1.0 \times 10^7$
4	Bacteria-1	995.2	70.6	12.4	1.5	20.6	$3.1 \times 10^5$
5	Non-bioaerosol-4	127.5	82.7	42.3	5.2	27.7	$3.9 \times 10^6$
6	Bacteria-2	1969.4	94.1	16.9	2.0	22.1	$3.6 \times 10^4$
7	Bacteria-3	1980.2	167.3	35.8	2.6	4.3	$3.8 \times 10^4$
8	Bacteria-4	2015.7	2038.6	832.8	8.4	11.3	$4.0 \times 10^3$
9	Fungal spores/pollen fragments-1	2015.7	2038.6	2037.1	13.2	49.7	$1.7 \times 10^2$
10	Fungal spores/pollen fragments-2	2015.7	2038.6	1653.1	14.0	9.6	$1.7 \times 10^3$
11	Bacteria-5	2015.7	2038.6	360.4	12.5	21.3	$1.1 \times 10^4$
12	Grass smut spores	67.7	2038.6	2037.1	7.8	13.6	$9.9 \times 10^2$

major clusters (i.e., any cluster with a population more than half of the average cluster size) from the average-linkage statistics. The oval circle in each panel of Fig. 3 indicates the point where  $R^2$  decreased significantly and RMS increased substantially, i.e., the optimum number of clusters was reached. The number of clusters identified on April 9, 15, 22, 30, and May 5 were 12, 12, 14, 10, 15, respectively. The detailed characteristics of the cluster centers on each individual day were tabulated in Table A.1–A.5. Here we classify the major types of clusters according to their relative fluorescence intensity, irregularity (i.e., AF), and size. According to the fluorescence signal intensities, they can be roughly divided into five classes: 1) weak in all three fluorescence channels; 2) relative strong in FL1\_280 but weak in the other two; 3) strong in FL1\_280 and FL2\_280 but weak in FL2\_370; 4) weak in FL1\_280 but strong in the other two; 5) strong in all three channels. They can be further classified according to their size and AF. Although the number of clusters and their relative abundance may vary from day to day, similar types of clusters can be found among different days. For example, the cluster 1 on April 15, the cluster 5 on April 22, the cluster 4 on April 30, and the cluster 3 on May 5 were very much the same as the cluster 4 on April 9. Similarity can also be found among the cluster 4 on April 15, the cluster 5 on April 22, the cluster 1 on April 30, the cluster 4 on May 5, and the cluster 6 on April 9. The cluster 9 on April 15, the cluster 12 on May 5, and the cluster 12 on April 9 all showed strong signals in channels FL2\_280 and FL2\_370. Accordingly, we classified all samples into 12 clusters and the cluster centers found on April 9 were used to represent the type of clusters of the field campaign period. Table 1 summarizes the details of the 12-cluster solution and the abundance of each cluster measured during this field work. These clusters were further identified according to their characteristic fluorescence signatures, size, and AF.

Clusters 1, 2, 3, and 5 were believed to be non-biological particles (i.e., non-bioaerosols) due to their low fluorescence signals and relatively high abundance (Robinson et al., 2013). Since the observation site is located within a few kilometers to the west of the industrial park and strong industry-related emissions have been often detected at the site (Ma et al., 2016; Zheng et al., 2015), it was reasonable to speculate that these weakly fluorescent non-bioaerosols were originated from the industrial park. This assumption was consistent with the rose-plot of non-bioaerosol concentration with respect to wind direction (see Fig. A.5), i.e., the high abundance of non-bioaerosol was mostly associated with easterly wind. Clusters 4, 6, 7, 8, and 11 all showed intense FL1\_280 or FL2\_280 signals but relative low FL2\_370 signal. This combination was consistent with the fluorescent feature of various kind of bacteria (Gabey et al., 2011), which tended to exist as aggregates or to be attached to the surfaces of other large particle in the atmosphere (Gorny et al., 1999). This also can explain the relatively large size associated with clusters 8 and 11 (8–12  $\mu\text{m}$ ). Although clusters 4, 6, 7, 8, and 11 all were bacteria, they differed substantially in FL2\_280 signal. This may be explained by the type of protein present in these bacteria. The 12th cluster was believed to be grass smut spores for its strong fluorescence in FL2\_370 channel and possessed a similar size range as reported by Healy et al. (2012a). Clusters 9 and 10 were characterized by their strong fluorescence in all three channels, which can be assigned to either fungal spores and/or pollens (Gabey et al., 2011). However, their sizes can differ from each other substantially. Typically, fungal spores ranged from 3 to 5  $\mu\text{m}$  but pollens were around 30  $\mu\text{m}$ , which in theory shall not be detected by the WIBS-4A in High Gain mode (0.8–15  $\mu\text{m}$ ). Nevertheless, Healy et al. (2012a) reported a size range of  $13.6 \pm 6.2 \mu\text{m}$  for pollens, which was within the detectible

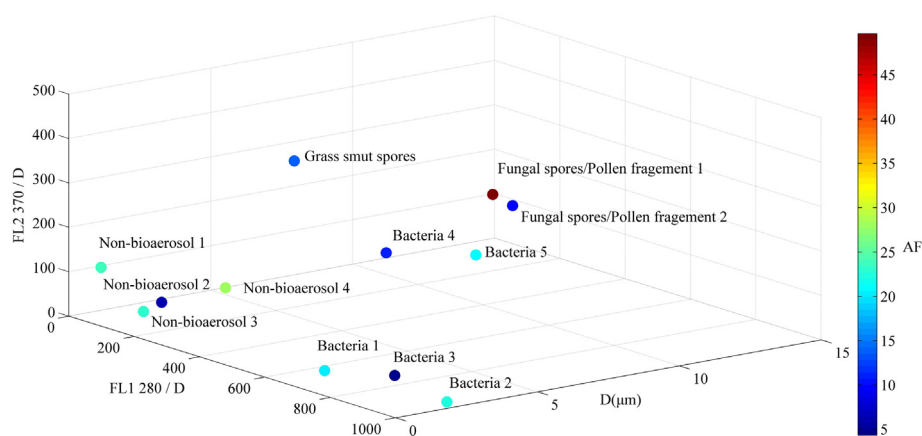


**Fig. 4.** Size-normalized fluorescence features of FL1\_280/D (y-axis) and FL2\_370/D (z-axis) plotted against particle aerodynamic diameter, D (x-axis) for each cluster. For the purpose of clarity only the median value for each cluster are presented. The color scale represents AF value, where navy-blue indicates a more spherical particle and red-brown represents a more asymmetrical particle.

range. Also, the large AF values indicated that these bioaerosols were significantly irregular in shape. Therefore, we attributed clusters 9 and 10 to fungal spores and/or pollen fragments.

Fig. 4 is the 4-D scatter plot of the 12 clusters identified in this work. Clearly, all non-bioaerosol particles, bacteria, and fungal spores and/or

pollen fragments are located within each individual cycle and grass smut spores stands alone from all other types of clusters, which further demonstrated that identification process mentioned above was indeed able to distinguish certain bioaerosol samples originating from different biological kingdoms (Healy et al., 2012a).

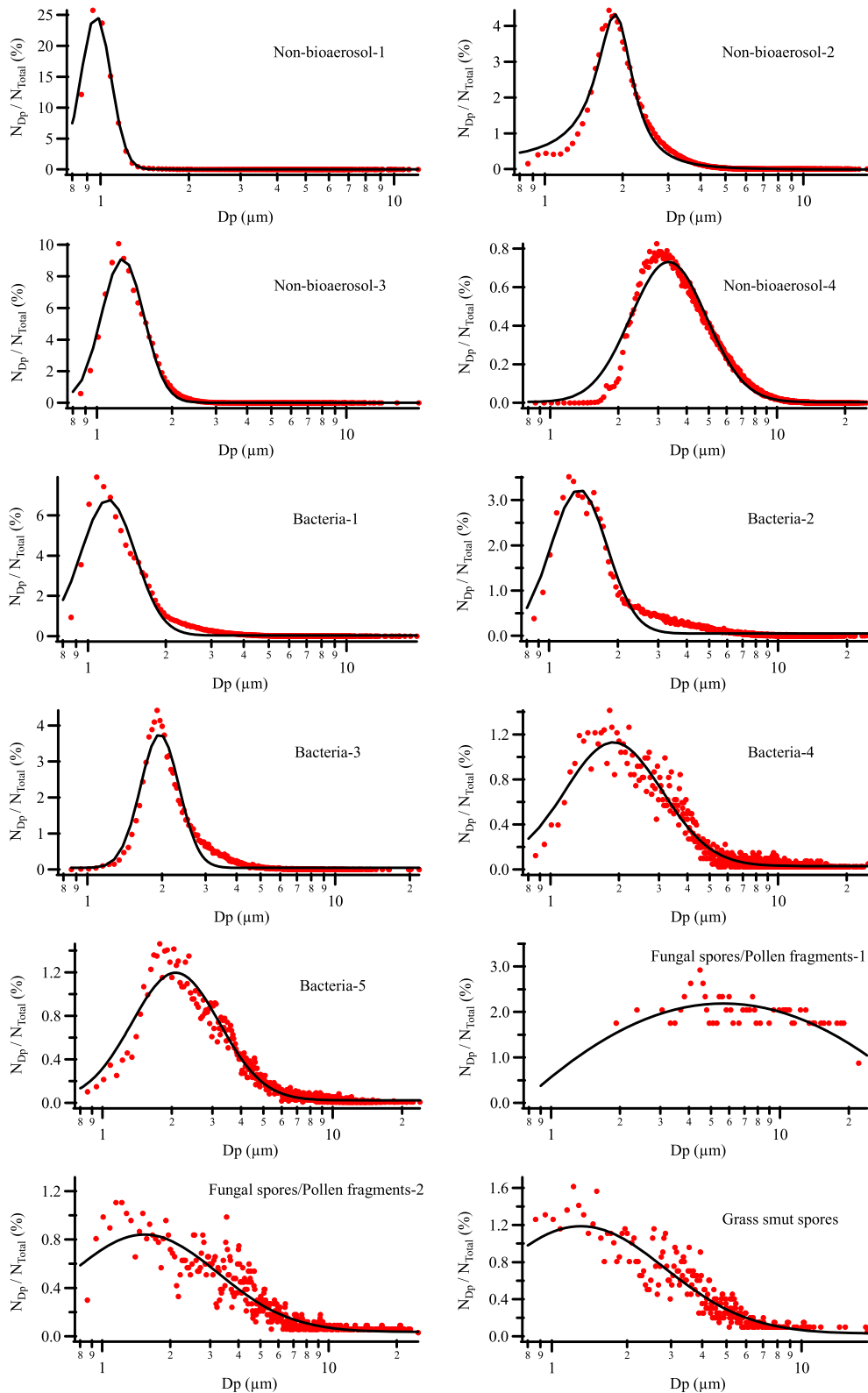


Fig. 5. Size-distributions of the 12-cluster solution, normalized by the abundance of the corresponding cluster ( $N_{Total}$ ).  $N_{Dp}$  is the number of particles in each  $Dp$  bin. The black curve in each panel is a monomodal lognormal fit.

3.4. Size and AF distributions of bioaerosols

Fig. 5 shows the number size-distributions of the 12 clusters of bioaerosols identified from this work. All non-bioaerosol clusters display monodispersed normal distributions, with a mean diameter ranging from 1 to 3.5  $\mu\text{m}$ . The shape of these distributions was

fundamentally the same as that of the ambient aerosols classified by a typical scanning mobility particle sizer (SMPS) or a APS, which indirectly verified that the HACA method can successfully identify and separate different size of non-biological particles from other bioaerosols. The mean sizes of all types of bacteria were around  $\sim 2 \mu\text{m}$ . The size distributions of bacteria tended to have longer and larger tails, not as

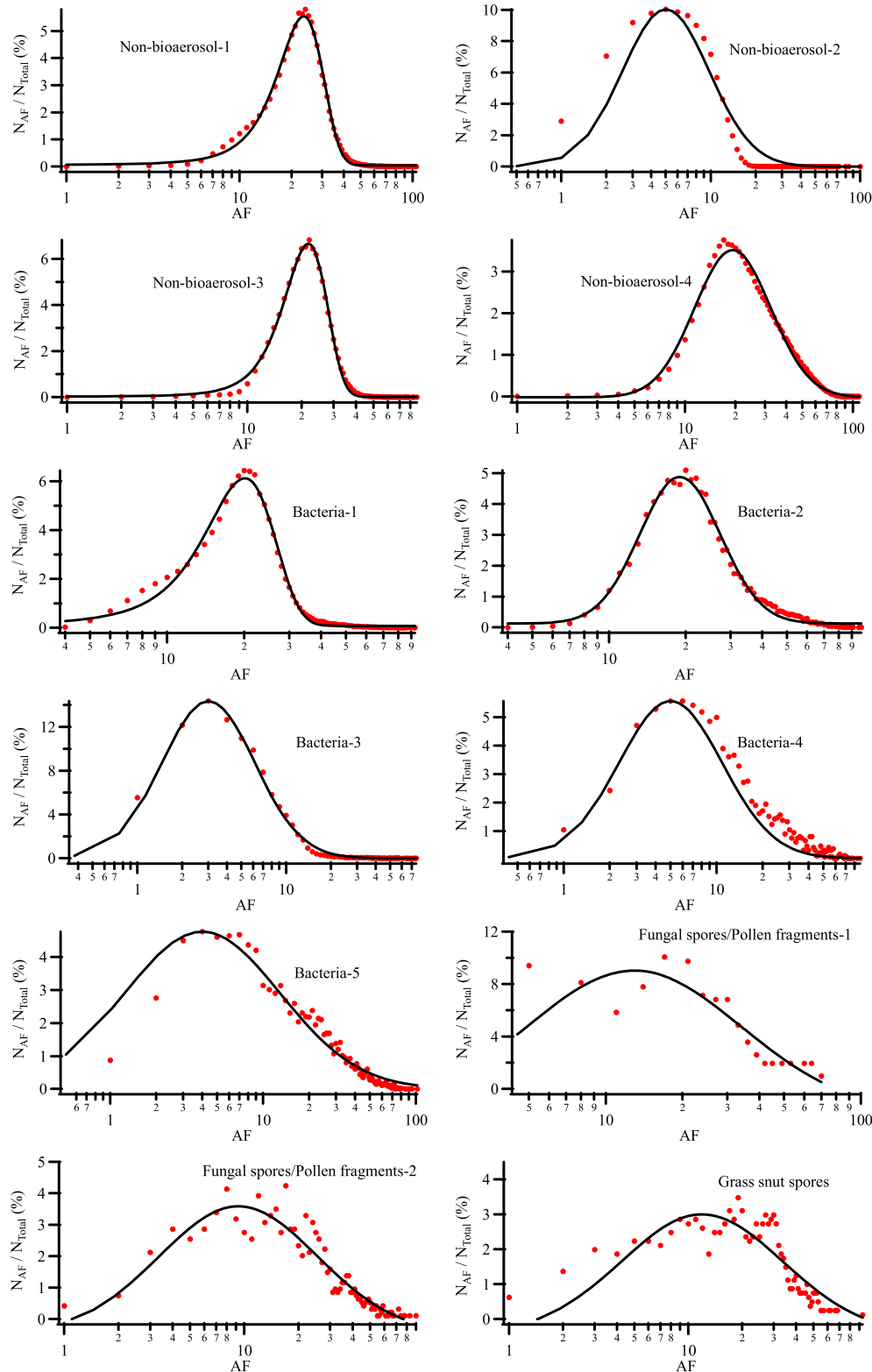


Fig. 6. AF-distributions of the 12-cluster solution, normalized by the abundance of the corresponding cluster ( $N_{Total}$ ).  $N_{AF}$  is the number of particles in each AF bin. The black curve in each panel is a monomodal lognormal fit.

normal as that of non-bioaerosol particles. Although individual bacterium is quite small in size, under ambient conditions bacteria often prefer to exist in aggregates, which can explain the relative large bacteria sizes identified by the HACA method. Moreover, bacteria were also found attached to the surfaces of other ambient particles, especially on larger particles with larger surface areas, which can explain the longer and larger tails present in the size distributions of bacteria and thus make these size distribution deviating from the normal distribution. The last three clusters of bioaerosols were either fungal spores and/or pollen fragments and showed the most irregular size distributions, with sizes ranging from  $\sim 1 \mu\text{m}$  to  $\sim 10 \mu\text{m}$ . Fungal spores can assume many structures and in fact fungi are often classified according to their spore-bearing structures. Before fungal spores detached from the mycelium, they can be straight, wave, or spiral in shape. Moreover, the shape of individual fungal spore can also be diverse, including round, oval, rod-shaped, cylindrical, or fusiform. Pollens are among the largest bioaerosols in the atmosphere. Since the WIBS-4A was operated in high gain mode, pollens were not likely detected in this work, except the fragments of pollen that can be smaller in size but very irregular in shape. All these properties of fungal spores/pollen fragments can explain the observed wide size range and the irregularity in size-distributions. It also can be noticed that the number concentrations of the fungal spores/pollen fragments were among the lowest of the 12 clusters, since larger particles tended to have a larger dry deposition rate.

Fig. 6 displays the distribution of all 12 clusters according their AF values, i.e., the irregularities. AF values of  $<30$  represent spherical shape; larger than 50 denote straight rod-shape; and anything in between 30 and 50 indicates irregular shape. AFs of most non-bioaerosols were around 20 to 30, i.e., very close to spherical shape, and particularly non-bioaerosol-2 has a AF of  $\sim 5.0$ , assuming a perfect spherical shape. Similar to the size-distributions, all bacteria-related clusters presented a relatively wide range of AF values (6–30), which was consistent with the fact that bacteria may present in the atmosphere as colonies with different sizes. Robinson et al. (2013) have reported that most bacteria AF values were in between 20–30, which was roughly in line with our results. Since our observation site was close to agriculture land and was quite humid during the spring time, it was providing an ideal environment for the evolving and reproduction of all kinds of bacteria. This can explain the fact that bacteria were the most abundant bioaerosols observed in this work, showing a wide range of shape factor. However, due to the complexity of the potential emission sources of bacteria, it would be impractical to identify the exact bacteria species according to their fluorescent signals alone. Although fungal spores/pollen fragments were much less than bacteria in concentration, they presented much more variety in morphology and clearly showed a multimodal AF-distributions (0–60), which were also consistent with the expected shape and morphology of fungal spores and pollen fragments.

### 3.5. Atmospheric implication

Although only a minor portion of the WIBS-4A measured signal can be attributed to real bioaerosols, the HACA results were consistent with the expected behavior of both bacteria and fungal spores/pollen fragments, indicating that HACA can be an effective method to retrieve bioaerosols information from the tremendous amount of data sets collected by the WIBS-4A. Despite the relatively small number concentration, bioaerosols still can play a significant role in the atmosphere. In this work, we found that the size range of bioaerosols can vary from  $\sim 1 \mu\text{m}$  up to  $\sim 10 \mu\text{m}$  and the shape of most bioaerosols were rather irregular, suggesting that bioaerosol may effectively promote heterogeneous ice nucleation by providing rough and irregular surfaces. The diurnal variation, especially the substantial decrease in concentration during the morning hours, was concurring with the swift development of boundary layer, indicating that vertical circulation can provide an effective channel to transport the surface-generated bioaerosols into the

upper troposphere. Therefore, the WIBS-4A measurements still can serve as a valuable method to quantify bioaerosols in the atmosphere and provide an insight into the IN budget in the atmosphere.

## 4. Conclusions

In this work, we have conducted on-line measurements of fluorescent aerosols near an industrial zone in the Yangtze River Delta region using a WIBS-4A instrument, operating in a high gain mode. HACA method was utilized to identify and speciate the potential bioaerosols from the measurement results. We found that majority of the particles detected by the WIBS-4A were non-fluorescent and thus non-biological in nature due to their extreme low fluorescent intensity (below the mean background fluorescent signals plus three times the standard deviation) and were excluded from further analysis. The daily average number of bioaerosols was around  $(1.0 \pm 0.3) \times 10^4$  counts, which accounted for only  $0.5 \pm 0.2\%$  of the WIBS-4A total signals and displayed a completely different diurnal profile from that of APS.

During HACA, each data point was treated as a five-membered vector (FL1\_280, FL2\_280, FL2\_370, size, AF) and the log-values of size and AF were used in the analysis. By maximizing the total distances among all potential cluster centers, a 12-cluster solution was accepted as the optimum result. These clusters were further identified according to their fluorescent signatures, size, and morphology, i.e., non-bioaerosol particles, bacteria, and fungal spores and/or pollen fragments. Bacteria and fungal spores and/or pollen fragments were the dominant bioaerosol species detected in this work.

The diurnal profiles of bioaerosols correlated very well with RH, reaching daily maxima around 3 AM to 6 AM, indicating the presence of humidity controlled bioaerosol emission mechanism, i.e., in springtime bacteria may flourish under moderate ambient temperature, relatively high humidity, and the absence of UV radiation. In general, the HACA results were in good agreement with the expected properties of bacteria and fungal spores and/or pollen fragments and can be demonstrated to be an effective way to retrieve real bioaerosol information from the WIBS-4A dataset. The size- and AF-distributions of bioaerosols indicated that bioaerosols normally varied substantially in size and assumed a rather irregular shape, suggested by the large AF values. Although the number concentration of bioaerosols was relatively small comparing to other atmospheric aerosols, most bioaerosols can efficiently serve as ice nuclei by providing rough and irregular surfaces, which was consistent with the ice nucleation mechanism (Demott and Prenni, 2010). Therefore, WIBS-4A measurements can still be informative for investigations of bioaerosols in the atmosphere, especially when HACA method was incorporated into the data processing. However, WIBS-4A can only provide very limited fluorescent information, i.e., only integrated fluorescent signals were collected, which strongly limited the potential of the instrument to speciate the bioaerosols. Although the detailed identity of a bioaerosol may not be necessary for the evaluation of its potential as ice nuclei, WIBS-4A equipped with a spectrometer detector may provide another dimension for bioaerosol analysis, which may be of great importance to investigate its health effect on the public.

## Acknowledgements

This work is supported by the National Key Research and Development Program of China (2017YFC0209501), National Natural Science Foundation of China (41730106 and 41575122). The data used here are listed in the tables, figures, and the supporting materials. The data used in this work are available from the authors upon request (zhengjun@nuist.edu.cn).

## Appendix A. Supplementary data

Supplementary data to this article can be found online at <https://doi.org/10.1016/j.scitotenv.2018.11.370>.

## References

- Cox, C.S., Wathes, C.M., 1995. *Bioaerosols Handbook*. CRC Press, Boca Raton, FL.
- Cross, E.S., Onasch, T.B., Ahern, A., Wrobel, W., Slowik, J.G., Olfert, J., et al., 2010. Soot particle studies instrument inter-comparison project overview. *Aerosol Sci. Technol.* 44, 592–611.
- DeMott, P.J., Prenni, A.J., 2010. New directions: need for defining the numbers and sources of biological aerosols acting as ice nuclei. *Atmos. Environ.* 44, 1944–1945.
- Després, V.R., Huffman, J.A., Burrows, S.M., Hoose, C., Safatov, A.S., Buryak, G., et al., 2012. Primary biological aerosol particles in the atmosphere: a review. *Tellus B* 64.
- Diehl, K., Matthias-Maser, S., Jaenicke, R., Mitra, S.K., 2002. The ice nucleating ability of pollen: part II. Laboratory studies in immersion and contact freezing modes. *Atmos. Res.* 61, 125–133.
- Everitt, B., 1993. *Cluster Analysis*. John Wiley & Sons, New York.
- Gabey, A.M., Stanley, W.R., Gallagher, M.W., Kaye, P.H., 2011. The fluorescence properties of aerosol larger than 0.8  $\mu\text{m}$  in urban and tropical rainforest locations. *Atmos. Chem. Phys.* 11, 5491–5504.
- Gorny, R.L., Dutkiewicz, J., Kryszynska-Traczyk, E., 1999. Size distribution of bacterial and fungal bioaerosols in indoor air. *Ann. Agric. Environ. Med.* 6, 105–113.
- Hairston, P.P., Ho, J., Quant, F.R., 1997. Design of an instrument for real-time detection of bioaerosols using simultaneous measurement of particle aerodynamic size and intrinsic fluorescence. *J. Aerosol Sci.* 28, 471–482.
- Healy, D.A., O'Connor, D.J., Burke, A.M., Sodeau, J.R., 2012a. A laboratory assessment of the waveband integrated bioaerosol sensor (WIBS-4) using individual samples of pollen and fungal spore material. *Atmos. Environ.* 60, 534–543.
- Healy, D.A., O'Connor, D.J., Sodeau, J.R., 2012b. Measurement of the particle counting efficiency of the "waveband integrated bioaerosol sensor" model number 4 (WIBS-4). *J. Aerosol Sci.* 47, 94–99.
- Heo, K.J., Kim, H.B., Lee, B.U., 2014. Concentration of environmental fungal and bacterial bioaerosols during the monsoon season. *J. Aerosol Sci.* 77, 31–37.
- IGAP, 1992. *The international global aerosol program*: Deepak publishing, Hampton, VA.
- Kaye, P.H., Barton, J.E., Hirst, E., Clark, J.M., 2000. Simultaneous light scattering and intrinsic fluorescence measurement for the classification of airborne particles. *Appl. Opt.* 39, 3738–3745.
- Ma, Y., Diao, Y., Zhang, B., Wang, W., Ren, X., Yang, D., et al., 2016. Detection of formaldehyde emissions from an industrial zone in the Yangtze River Delta region of China using a proton transfer reaction ion-drift chemical ionization mass spectrometer. *Atmos. Meas. Tech.* 9, 6101–6116.
- O'Connor, D.J., Healy, D.A., Sodeau, J.R., 2013. The on-line detection of biological particle emissions from selected agricultural materials using the WIBS-4 (waveband integrated bioaerosol sensor) technique. *Atmos. Environ.* 80, 415–425.
- O'Connor, D.J., Healy, D.A., Hellebust, S., Buters, J.T.M., Sodeau, J.R., 2014. Using the WIBS-4 (waveband integrated bioaerosol sensor) technique for the on-line detection of pollen grains. *Aerosol Sci. Technol.* 48, 341–349.
- Panne, U., Knoller, A., Kotzick, R., Niessner, R., 2000. On-line and in-situ detection of polycyclic aromatic hydrocarbons (PAH) on aerosols via thermodesorption and laser-induced fluorescence spectroscopy. *Fresenius J. Anal. Chem.* 366.
- Pöhlker, C., Huffman, J.A., Pöschl, U., 2012. Autofluorescence of atmospheric bioaerosols – fluorescent biomolecules and potential interferences. *Atmos. Meas. Tech.* 5, 37–71.
- Pope, F.D., 2010. Pollen grains are efficient cloud condensation nuclei. *Environ. Res. Lett.* 5, 044015.
- Poschl, U., 2005. Atmospheric aerosols: composition, transformation, climate and health effects. *Angew. Chem. Int. Ed.* 44, 7520–7540.
- Poschl, U., Shiraiwa, M., 2015. Multiphase chemistry at the atmosphere-biosphere interface influencing climate and public health in the anthropocene. *Chem. Rev.* 115, 4440–4475.
- Poschl, U., Martin, S.T., Sinha, B., Chen, Q., Gunthe, S.S., Huffman, J.A., et al., 2010. Rainforest aerosols as biogenic nuclei of clouds and precipitation in the Amazon. *Science* 329, 1513–1516.
- Reid, C.E., Gamble, J.L., 2009. Aeroallergens, allergic disease, and climate change: impacts and adaptation. *EcoHealth* 6, 458–470.
- Robinson, N.H., Allan, J.D., Huffman, J.A., Kaye, P.H., Foot, V.E., Gallagher, M., 2013. Cluster analysis of WIBS single-particle bioaerosol data. *Atmos. Meas. Tech.* 6, 337–347.
- Toprak, E., Schnaiter, M., 2013. Fluorescent biological aerosol particles measured with the waveband integrated bioaerosol sensor WIBS-4: laboratory tests combined with a one year field study. *Atmos. Chem. Phys.* 13, 225–243.
- Yu, X., Wang, Z., Zhang, M., Kuhn, U., Xie, Z., Cheng, Y., et al., 2016. Ambient measurement of fluorescent aerosol particles with a WIBS in the Yangtze River Delta of China: potential impacts of combustion-generated aerosol particles. *Atmos. Chem. Phys. Discuss.* 2016, 1–31.
- Zheng, G., He, K., Duan, F., Cheng, Y., Ma, Y., 2013. Measurement of humic-like substances in aerosols: a review. *Environ. Pollut.* 181, 301–314.
- Zheng, J., Ma, Y., Chen, M., Zhang, Q., Wang, L., Khalizov, A.F., et al., 2015. Measurement of atmospheric amines and ammonia using the high resolution time-of-flight chemical ionization mass spectrometry. *Atmos. Environ.* 102, 249–259.